Outer Hair Cell Function is Normal in βV Spectrin Knockout Mice.

Michael C. Stankewich[1*], Jun-Ping Bai[2*], Paul R. Stabach[1], Saaim Khan[3], Lei Song[4], Jon S. Morrow[1,5], Joseph Santos-Sacchi[6,7,8], Dhasakumar S. Navaratnam[2,6,7 ^]

1 Department of Pathology, Yale School of Medicine, New Haven, CT, U.S.A

2 Department of Neurology, Yale School of Medicine, New Haven, CT, U.S.A

3 Cranbrook Kingswood Upper School, MI, USA

4 Department of Otolaryngology-Head and Neck Surgery, Shanghai Ninth People's Hospital, Shanghai Jiaotong University School of Medicine, Shanghai, China

5 Department of Molecular, Cellular, and Developmental Biology, Yale University, New Haven, CT, U.S.A

6 Department of Surgery, Yale School of Medicine, New Haven, CT, U.S.A

7 Department of Neurobiology, Yale School of Medicine, New Haven, CT, U.S.A

8 Department of Cellular and Molecular Physiology, Yale University, New Haven, CT, U.S.A

* Co-first authors
^ Corresponding Author

Address correspondence to Dr. Dhasakumar Navaratnam
Yale School of Medicine, Department of Neurology, PO Box 208018,
New Haven, CT., 06519
email: dhasakumar.navaratnam@yale.edu

Keywords: cochlea, auditory brainstem response, electromotility, distortion product otoacoustic emissions, Spnb5, ribbon synapse, cochlear nerve

ABSTRACT

Reports have proposed a putative role for βV spectrin in outer hair cells (OHCs) of the cochlea. In an ongoing investigation of the role of the cytoskeleton in electromotility, we tested mice with a targeted exon deletion of βV spectrin (Spnb5), and unexpectedly find that Spnb5$^{(-/-)}$ animals' auditory thresholds are unaffected. Similarly, these mice have normal OHC electromechanical activity (otoacoustic emissions) and non-linear capacitance. Moreover, Spnb5 mRNA is undetectable in the organ of Corti or OHCs. In contrast, magnitudes of auditory brainstem response (ABR) peak 1-amplitudes are significantly reduced. Evidence of a synaptopathy was absent with normal hair cell CtBP-2 counts. In Spnb5$^{(-/-)}$ mice, the number of afferent and efferent nerve fibers is decreased. Taken together, these data establish that βV spectrin is important for hearing, affecting neuronal structure and function. Significantly, these data exclude βV spectrin as functionally important to OHCs as has been previously suggested.

INTRODUCTION

In the early 1990s, several groups made key seminal observations of a spectrin/actin lattice in the cochlear outer hair cells (OHCs) (Holley & Ashmore, 1990) (Holley, Kalinec, & Kachar, 1992). Their electron micrographs propelled an exquisite model of the spectrin/actin lattice assembled just beneath the OHC lateral membrane with longitudinal spectrin molecules linked to circumferential actin filaments that, in turn, were linked to the plasma membrane by electron-dense pillars. Their work also identified a pool of spectrin in the actin-rich cuticular plate. Another study evaluated spectrin proteins in cochlear innervation during rodent development (Hafidi, Despres, & Romand, 1990). They identified differences in developmental expression of the erythroid beta spectrin (Spnb1 spectrin) compared to the most ubiquitous nonerythroid form αII/ βII spectrin, similar to what is observed in the brain. What is not certain from these earlier studies is the specific spectrins involved, a family now known to consist of two alpha spectrins (Spna1 and 2) and five beta spectrins (Spnb1-5). More recently, it has been shown that Spnb4 is restricted to the nodes of Ranvier in myelinated axons and is also a deafness-related gene (Parkinson et al., 2001) (Lewis et al., 2018). It appears from these studies that the deafness in the quivering mouse is likely not originating in the cochlea but rather is central in origin. Furthermore, Spnb2 spectrin, when selectively deleted from the mouse cochlea sensory epithelia by crossing Spnb2 floxed mice with Atoh-1 Cre-recombinase, causes profound deafness due to a disruption of the stereocilia rootlets in the cuticular plate in hair cells (Liu et al., 2019). Thus, the function of specific spectrins,

77 particularly as it relates to the OHC lateral membrane and cochlear innervation,
78 remains unclear. In humans, the molecule βV spectrin (SPTBN5) that was first
79 discovered in the retina, is involved with the retinal disorder, Usher syndrome
80 (Stabach & Morrow, 2000) (Papal et al., 2013). Further reports have proposed a
81 putative role for βV spectrin in a second sensorineural function, hearing. One
82 group's observations demonstrated that antisera raised against the C-terminal
83 peptide of SPTBN5, the largest form of spectrin, and an orthologue of beta(Heavy)
84 spectrin in Drosophila, labeled structures along the lateral membrane of the OHC
85 (Legendre, Safieddine, Kussel-Andermann, Petit, & El-Amraoui, 2008) (Cortese et
86 al., 2017). This observation drew attention because detection of this giant spectrin
87 in tissue other than retina and testis has been elusive. This finding raised the
88 possibility that βV spectrin was involved in the electromotile properties of OHCs.
89 Continuing an ongoing effort in our lab to define the cytoskeleton's role in
90 electromotility, we sought to determine the role of βV spectrin in OHC function (Bai
91 et al., 2010). In this study, we analyzed βV spectrin expression in the cochlea and
92 addressed its function in mice with a targeted deletion of Spnb5. We tested hearing
93 by auditory brainstem response (ABR), measured OHC-mediated otoacoustic
94 emissions and OHC nonlinear capacitance (NLC), and evaluated the number of
95 inner hair cell (IHC) ribbon synapses and nerve fibers that innervate the cochlear
96 sensory epithelium. We find that while OHC function is unaffected in the absence
97 of βV spectrin, nerve counts are reduced at the habenular, in all three turns of the
98 cochlea, and in efferent fibers in the mid and basal turns, which collectively account
99 for the reduced wave I amplitudes in ABRs. We conclude that βV spectrin is

necessary to maintain the integrity or function of afferent and efferent nerves of the peripheral auditory system, but plays no role in the OHC itself.

RESULTS

Mouse βV spectrin amino acid sequence is divergent from the human protein.

Surprisingly, a sequence alignment comparing the mouse amino acid sequence to the human amino acid sequence reveals a significant divergence. In contrast, other beta spectrins, including beta I-IV, have ~ 90% amino acid conservation between human and mouse sequences. By aligning human and mouse βV spectrin, we note a significant divergence at the N- and C-termini of the proteins and an internal stretch of amino acids from position 817-922 (**Figure 1A**). Of note is that the initiator methionine residue in the human form is conserved between mouse and human genes and lies at position 36 and within exon 2 (**Figure 2**). The mouse sequence incorporates an unusual homorepeat of glutamines and, notably, does not have a bona fide pleckstrin homology (PH) domain seen in the human form.

Spnb5 mRNA tissue expression.

Spnb5 spectrin is expressed in most mouse tissues but at low levels. In ENCODE, the level of Spnb5 transcripts is an order of magnitude less abundant than the ubiquitous form Spnb2 (**Figure 1B**) (Yue et al., 2014). The peak abundance of Spnb2 approaches 50 RPKM while Spnb5 is 0.5 RPKM in testis (**Figure 1B, C**). Interestingly, the GTEX dataset shows high expression of Spnb5 in the peripheral (tibial) nerve (**Figure 1D**). To validate that mRNA is detected in mice, we tested RNA from the testis with primer sets that bridged exons. By standard rt-PCR, Spnb5 mRNA fragments encoding both the N-terminus and C-terminus were

128 amplified from testis and brain RNA, and its identity was confirmed by Sanger
129 sequencing. In contrast to brain and testicular tissue, we could not detect Spnb5
130 mRNA in isolated OHCs and whole organ of Corti by both conventional and nested
131 PCR (Table 1 details the gene-specific primer sets). Using rt-PCR from ~3000
132 OHCs and organ of Corti, we detect both Spnb1 and Spnb2. Using nested PCR,
133 amplicons for these spectrins are robust, while we do not visualize any product for
134 Spnb5 (**Figure 1E**). These data are in accord with data derived from the public
135 data sets of transcriptome profiling for OHCs in gEAR (https://umgear.org/) (**See**
136 **supplementary Figure1**).
137

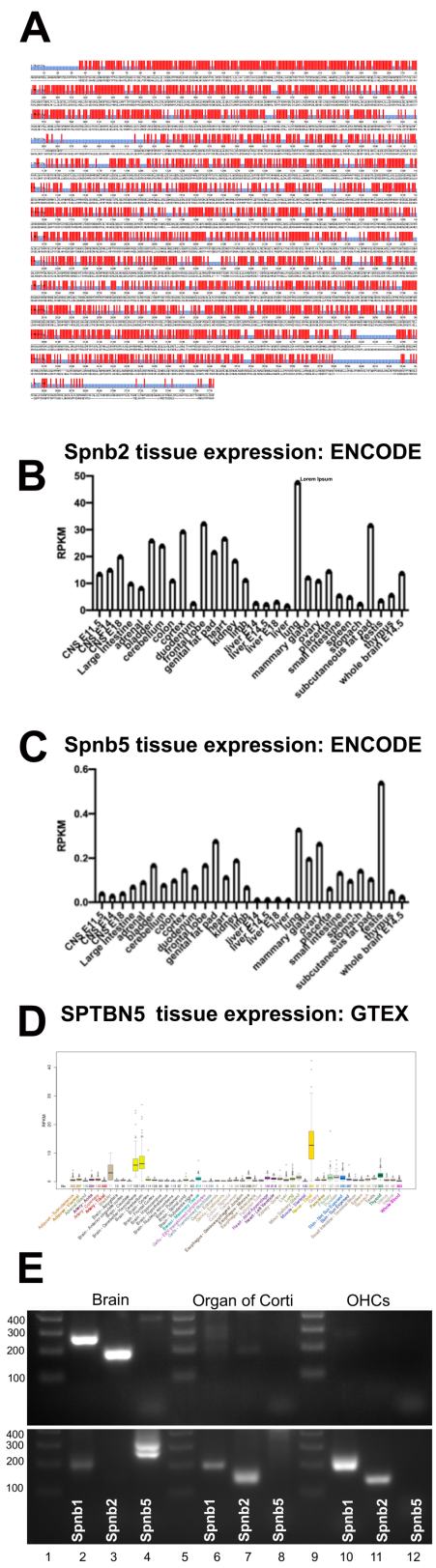

Figure 1. (A) Spnb5 amino acid sequence differs from humans. Shown is the comparison of the deduced amino acid sequence of mouse and human Spnb5. Conserved amino acids are marked in red. There is divergence at the N and C termini. In addition, a region in the middle of the protein from posiiton 817-922 shows significant divergence. The mouse version of this gene shares only 65.6 percent identity with the human form. **(B, C) Spnb5 is expressed in brain and testis.** The relative abundance of Spnb2 transcripts as compared to Spnb5 in mouse tissues. Shown are the expression of Spnb2 and 5 in RNA Seq. NCBI reference datasets (ENCODE; Bioproject PRJNA66167_(Yue et al., 2014). On average, the abundance of Spnb5 mRNA is an order of magnitude less abundant than Spnb2. Of the tissues examined, adult testis has the most mRNA for Spnb5. **(D) In human, Spnb5 is most expressed in peripheral nerve.** The relative abundence of Spnb5 in different tissues in GTEX database is presented (version 6) (Consortium, 2013). Of all the tissues examined Spnb5 is expressed in highest amounts in the peripheral nerve (tibial nerve). **(E) Spnb5 mRNA is not detectable in the organ of Corti or OHCs.** Shown are PCR amplifications from mouse brain (lanes 2-4), organ of Corti (lanes 6-8) and OHCs (lanes 10-12) of Spnb1 (lanes 2, 6 and 10), Spnb2 (lanes 3, 7 and 11) and Spnb5 (lanes 4, 8 and 12). The upper panel shows amplicons for these three mRNA transcripts using outer primers while the lower panel shows amplicons of primers using a nested set of primers. All three spectrins are detectable in brain. Spnb1 and 2 are detectable in both the organ of Corti and OHCs (lanes 6-7 and 10-11). Spnb5 however, is not detectable using either primer set (lanes 8 and 12).

Figure 1

139 **Supplementary Figure 1.**

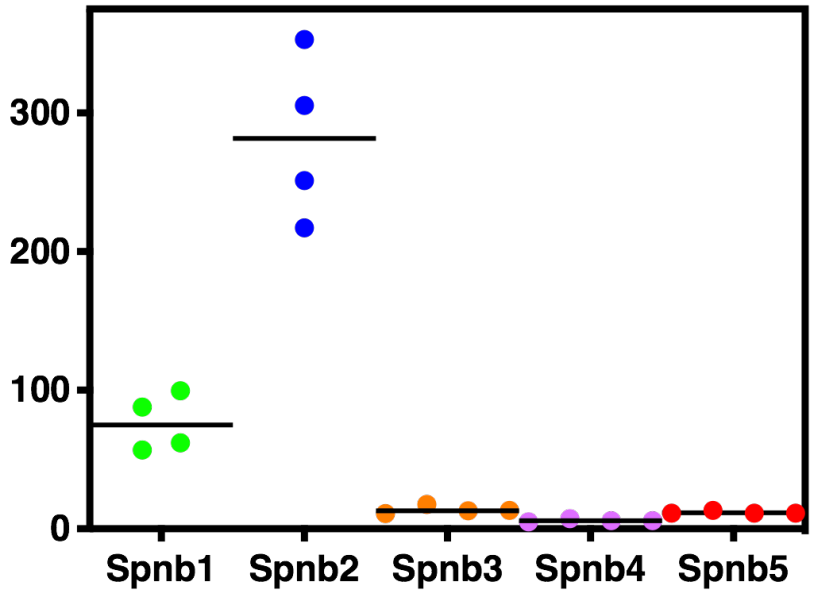

140
141 **Expression levels for each of the beta spectrins in OHCs.**
142 Mining data from the gene Expression Analysis Resource (gEAR) we graphed the
143 abundance of each of the five beta spectrin genes. This data set was derived from
144 transcriptome analysis using sc-RNAseq of cell populations isolated from mouse
145 cochleae (Li et al., 2018).
146
147 **Targeted knockout of Spnb5 in mice using homologous recombination.**

148 In order to properly target the βV spectrin gene in mice, we needed to know its
149 precise gene structure. While the human gene has been well characterized and
150 indexed since its discovery in 2000 (Stabach & Morrow, 2000), there has been
151 ambiguity in the intron/exon usage in the mouse gene found on chromosome 2.
152 The GENBANK entry for Spnb5 has been modified many times in the last several
153 years, with the last significant annotation in 2007 (Benson et al., 2013). This
154 annotation was derived by automated computational analysis using gene
155 prediction algorithms. The exon prediction is made difficult because 1) the gene is
156 very large, so PCR amplifying a full-length cDNA is not trivial, and 2) the
157 conservation between human and mouse intron/exon boundaries is weak at the N-

158 and C-termini. The current and accepted annotated version in both the UCSC
159 genome browser and in Ensembl shows Spnb5 spectrin mRNA in the mouse to be
160 14.4 kb with a 10,872 bp ORF that has 66 exons and codes for 3623 amino acids:
161 NM_001370938: NP_001357867.1. This version has been validated in the
162 ENCODE project based on the robustness of next-generation sequencing efforts
163 over the last several years (Yue et al., 2014).
164
165 Shown in the schematic in **Figure 2A** is the strategy for targeted deletion of exon
166 2 of Spnb5. The knockout strategy was based on the transcript ID:
167 ENSMUST00000156159.3, and a targeting construct was generated in which
168 three Lox P sites were inserted to flank the neomycin selection marker and exon
169 2 containing the start codon, resulting in disruption of the open reading frame upon
170 Cre-mediated excision. Exon 2 contains the ATG start codon (with a consensus
171 Kozak sequence) and an additional 37 amino acids at its N-terminus. Notably, the
172 codon for the methionine residue corresponding to the human start codon is also
173 contained within the second exon. A genomic bacterial artificial chromosome
174 containing the Spnb5 locus was obtained, and genomic DNA fragments containing
175 the first exons of Spnb5 were subcloned in pEasy (a gift from Sankar Ghosh). The
176 targeting vector comprised a 4.3 kb long arm, a 4.1 kb short arm, and a middle
177 selection cassette which contains exon two flanked by a PGK–neomycin
178 resistance (Neo), two FRT sites, and the herpes simplex thymidine kinase gene
179 (**Figure 2B and Primer Sets in Table 2**). The targeting plasmid DNA was
180 linearized with Cla1 and electroporated into mouse embryonic stem cells (ESCs)

181 (129SV/EV). ESCs were selected for neomycin/G418 resistance. Positive clones
182 were identified by PCR and confirmed by Southern blot analysis using external
183 and internal probes. A correctly targeted ESC clone was injected into C57BL/6J
184 blastocysts to produce germline transmitting chimeric mice. These were then
185 mated with actin-Cre C57BL/6J transgenic mice for generation of heterozygous
186 Spnb5 transgenic mice with both the Neo cassette and exon two removed
187 (Spnb5$^{(+/-)}$). The resulting Spnb5$^{(+/-)}$ offspring were crossed to generate βV
188 spectrin-deficient mice. The genotypes of these mice were confirmed by PCR
189 amplification (**Figure 2C**). Chimeric mice were backcrossed onto the C57BL/6J
190 strain. Litters from heterozygous breeders Spnb5$^{(+/-)}$ / Spnb5$^{(+/-)}$ were of normal
191 number, and the mice of all genotypes were phenotypically indistinguishable with
192 normal lifespans >2 yrs old. We confirmed decreased expression of Spnb5 in
193 cDNA from testes of Spnb5$^{(-/-)}$ mice, where we found equivalent expression of
194 Spnb2 and Spna2 (**Figure 2D and Primer Sets in Table 3)**.
195

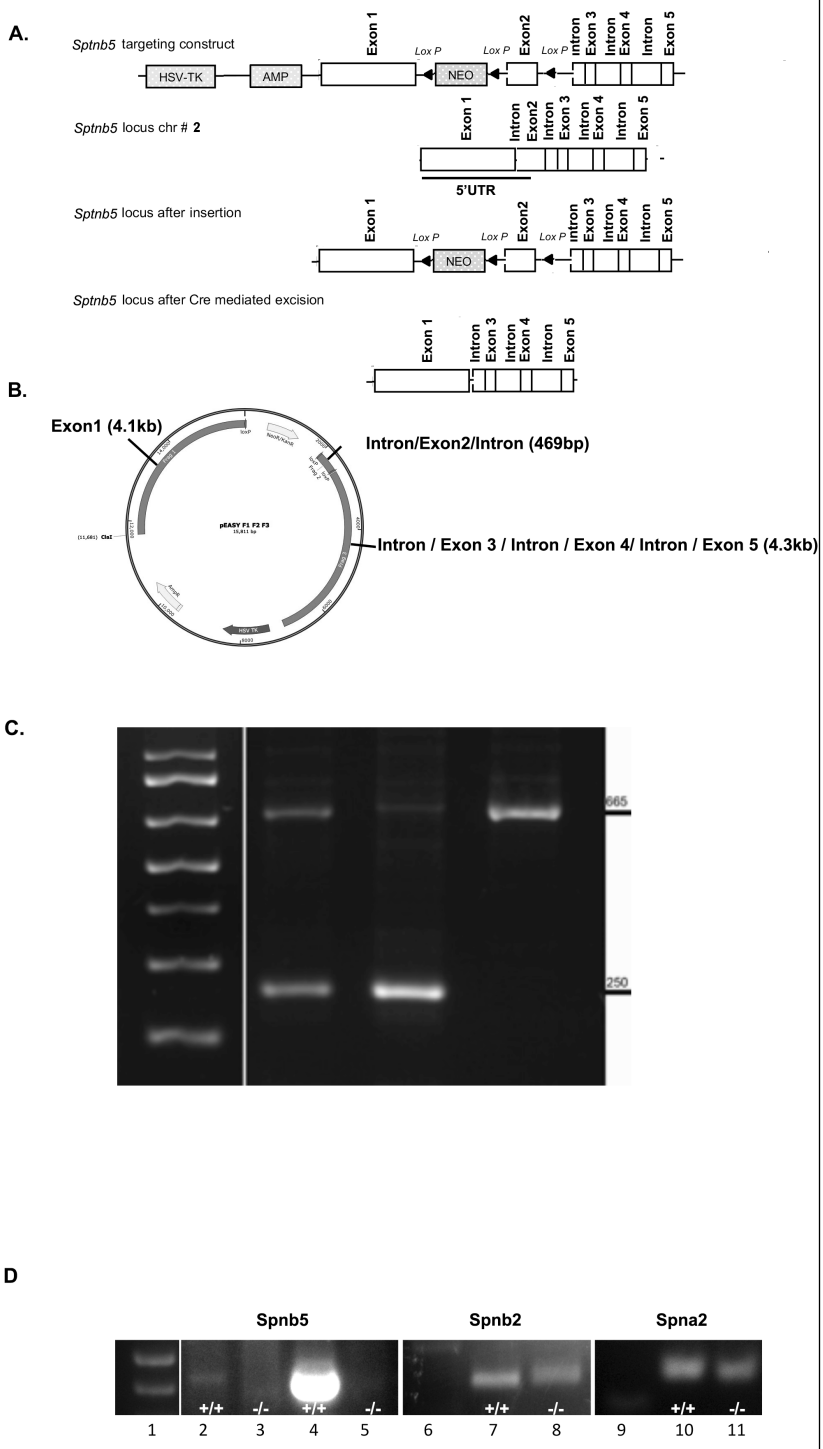

Figure 2. Exon 2 of the Spnb5 gene was removed using homologous recombination. (A) Schematic of the strategy used to delete exon 2. The construct contained a short arm of exon 1 and a long arm of exons 3, 4, and 5 together with the intervening introns. Both the selection marker Neo and exon two are flanked by Lox P sites. Linearized plasmid was injected into ES cells and clones with homologous recombination and selected by neomycin (Neo)/ G418 resistance. Mice were then crossed with Actin-Cre mice to generate floxed mice lacking the Neo cassette and exon 2. **(B) Vector map of pEASY used to target Spnb5 deletion.** Exon 2 was subcloned between two Lox P sites adjacent to the Neo gene. These two genomic fragments were in turn placed between a 4.1kb short arm containing Exon 1 and a 4.3kb long arm containing exons 3, 4, and 5 and the intervening introns. The vector also contains a thymidine kinase and ampicillin gene allowing for selection. The plasmid was linearized with Cla1. **(C) PCR amplification of genomic DNA confirming deletion of exon two and flanking intronic sequence.** In genomic DNA from Spnb5$^{(-/-)}$ mice**,** primers that amplify a product no longer contain part of intron 1; exon 2; and part of intron 2/3. Lane 1 base pair standards, lane 2 Spnb5$^{(+/-)}$, lane 3 Spnb5$^{(-/-)}$, lane 4 Spnb5$^{(+/+)}$. The larger fragment of 665 bp consists of unexcised exon two while the smaller fragment consists of genomic DNA fragment from which exon two has been excised. **(D) Decreased expression of Spnb5 in Spnb5$^{(-/-)}$ testicular cDNA compared to Spnb2 and Spna2**. Spnb5 exons 58-60 in lanes 2-3, Spnb5 exon 53-55 in lanes 4-5; Spnb2 in lanes 7-8 (exons 28-29) and Spna2 (exons 54-55) in lanes 10-11**.** WT in lanes 2, 4, 7 and 10. Spnb5$^{(-/-)}$ in lanes 3, 5, 8 and 11.

Figure 2

197 **Auditory thresholds and OHC function are similar between Spnb5$^{(-/-)}$ and**
198 **control mice.**
199 To investigate how the loss of Spnb5 impacts auditory information processing, we
200 compared the *in vivo* ABR of 2-month-old Spnb5$^{(+/+)}$ and Spnb5$^{(-/-)}$ mice. ABR
201 thresholds were not altered in Spnb5$^{(-/-)}$ mice at all sound frequencies tested from
202 2 to 32 kHz (**Figure 3A**). We also found that distortion product otoacoustic
203 emissions (DPOAE) measurements, a measure specific to OHC function, are not
204 affected by the loss of βV spectrin (**Figure 3B**). These findings with preserved
205 DPOAE thresholds also extended to suprathreshold responses at sound
206 intensities of 80-90 dB SPL (**Figure 3C**). Since spectrins have been implicated in
207 membrane integrity and protein shuttling, we also assayed prestin expression in
208 the lateral wall using its gating charge movement (NLC) at postnatal day 13 (when
209 prestin expression increases in OHCs) and at two months (Abe et al., 2007). At
210 both these time points, we found NLC to be unaffected in Spnb5$^{(-/-)}$ mice (**Figure**
211 **4A**). Our measures of the different parameters of NLC, Q_{sp}, V_h, and z, were similar
212 between WT and Spnb5$^{(-/-)}$ mice (**Figure 4, A-D**).

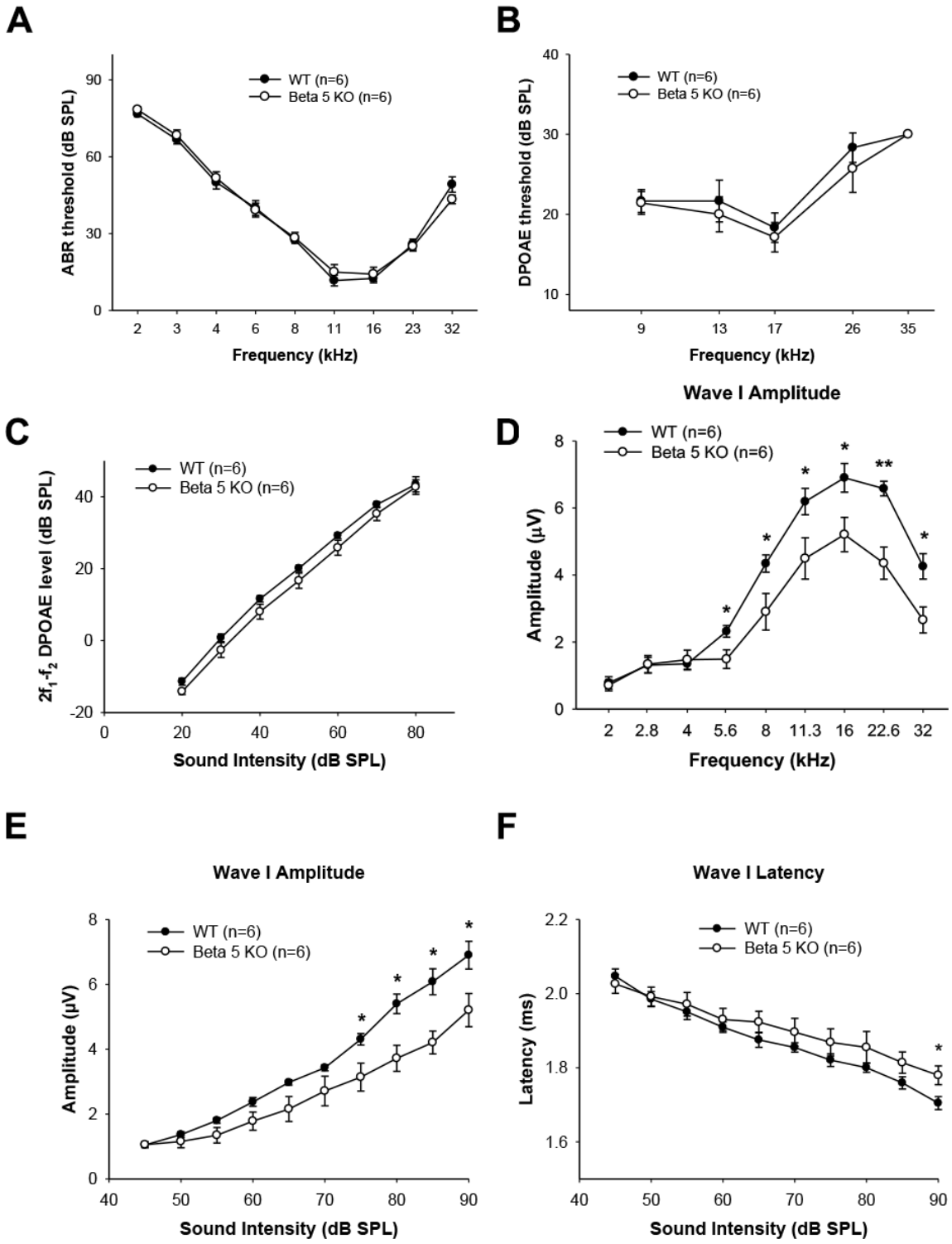
A
WT (n=6)
Beta 5 KO (n=6)
ABR threshold (dB SPL)
Frequency (kHz)
B
DPOAE threshold (dB SPL)
Frequency (kHz)
C
2f1-f2 DPOAE level (dB SPL)
Sound Intensity (dB SPL)
D
Wave I Amplitude
Amplitude (µV)
Frequency (kHz)
E
Wave I Amplitude
Amplitude (µV)
Sound Intensity (dB SPL)
F
Wave I Latency
Latency (ms)
Sound Intensity (dB SPL)

213 **Figure 3**

Figure 3. ABR analysis suggests a neuronal and not OHC dysfunction in Spnb5$^{(-/-)}$ mice. (A) thresholds at frequencies from 2-32 kHz reveal no change in Spnb5$^{(-/-)}$ mice. ABR thresholds in Spnb5$^{(-/-)}$ (open circle) and littermate WT (solid circle) mice at 2-month-old are plotted over a range of frequencies. There was not a significant difference between WT and Spnb5$^{(-/-)}$ mice at all frequencies tested from 2 to 32 kHz. **(B) Similar DPOAE thresholds were observed in 2-month-old WT and Spnb5$^{(-/-)}$ mice at all frequencies**. **(C) DPOAE input/output function are unaffected in Spnb5$^{(-/-)}$ mice.** Input/output (I/O) function analysis of DPOAE responses in WT (solid circle) and Spnb5$^{(-/-)}$ (open circle) mice as a function of sound intensity at 16 kHz at two months of age are graphed. DPOAE amplitudes in Spnb5$^{(-/-)}$ mice showed no significant difference across all sound intensities compared to WT mice. **(D) Wave I amplitudes are significantly altered between Spnb5$^{(-/-)}$ and WT at high stimulus intensities at frequencies 5.6-32 kHz, but not at frequencies 2-4 kHz.** Shown is the wave I amplitudes at 90 dB SPL. There is a consistent reduction in the amplitudes of wave I amplitudes at these suprathreshold intensities from 5.6-32 kHz. **(E) Wave I amplitudes were significantly reduced in Spnb5$^{(-/-)}$ mice at higher sound intensities (75-90 dB SPL). (F) Wave I latencies at 16 kHz show significant delays at 90 dB SPL.** Latencies at all other frequencies are not significantly delayed (data not shown). Data are means +/- SEM. The number (n) of animals per experiment is shown in each graph. Asterisks indicate $P<0.05$.

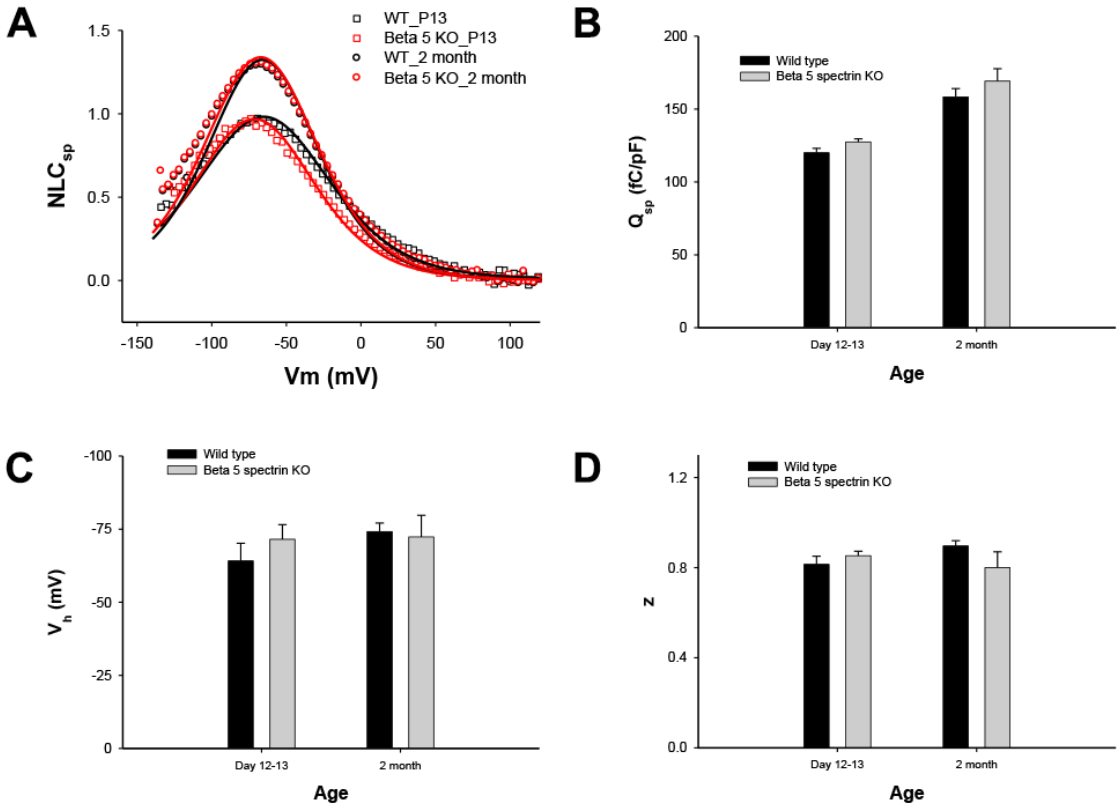

Figure 4

Figure 4. Spnb5$^{(-/-)}$ mice have similar nonlinear capacitance characteristics as controls at two age groups. NLC was measured at postnatal day 13, a midpoint of NLC development, and at two months when hearing is mature. **(A) There are no significant effects of OHC NLC in Spnb5$^{(-/-)}$ mice.** Shown are representative traces of NLC measurement in Spnb5$^{(-/-)}$ and WT mice. There are no differences in NLC between Spnb5$^{(-/-)}$ and WT mice at these two time points. **B, C, and D. NLC parameters are unaffected in Spnb5$^{(-/-)}$ mice.** Shown are means (+/- SEM) of NLC parameters in Spnb5$^{(+/+)}$ and Spnb5$^{(-/-)}$ mice at 13 days and two months, with no significant differences (P>0.05) in all of these measures (Q_{sp}, V_h and z). **(B) Q_{sp}, a specific measure of net charge movement per unit of membrane corrected for linear capacitance. (C) V_h, a measure of the voltage dependence of charge movement. (D) z, a measure of the slope in NLC voltage dependence and indicative of the unitary charge movement.**

249 **Loss of βV spectrin affects hearing sensitivity in a manner suggesting a**
250 **neural processing disorder.**
251 The ABR is characterized by a series of electrical waves representing the
252 progressive transfer of the auditory signal from the periphery to the CNS (Song,
253 McGee, & Walsh, 2006). Wave I represents the summated response from the
254 spiral ganglion and auditory nerve (Melcher et al., 1996). While we see no
255 differences in ABR thresholds, we note that Wave I amplitudes from 5.6 kHz and
256 upwards are significantly altered between Spnb5$^{(-/-)}$ and WT at high stimulus
257 intensities (suprathreshold). We also analyzed the latency of wave I to investigate
258 any potential changes in the rate of propagation of neural transmission (**Figure 5**).
259 Wave I latency at 16 kHz was progressively delayed at high sound intensities
260 reaching significance at the highest sound intensity (90 dB SPL). Latencies at other
261 frequencies were not significantly different from WT.
262
263 **Spnb5 plays a critical role in sensorineural processing.**
264 What could be the cause of the differences in amplitudes of wave I between WT
265 and Spnb5$^{(-/-)}$ mice? We sought to exclude synaptopathy as a cause of the
266 decrease in wave I amplitudes. For instance, spectrins have been shown to be
267 important in targeting structural elements of the synaptic apparatus as well as
268 maintaining the integrity and compartmentalization of axons and dendrites
269 ((Hammarlund, Jorgensen, & Bastiani, 2007), (Stankewich et al., 2010), (Efimova
270 et al., 2017; Stankewich et al., 2011), (Lorenzo et al., 2019). We compared the
271 numbers of ribbon synapses at the base, middle, and apex of the organ of Corti

272 between Spnb5$^{(-/-)}$ and WT mice. We used antibody labeling of the marker protein
273 CtBP-2 (Bramhall, McMillan, Kujawa, & Konrad-Martin, 2018), a major component
274 of the ribbon synapses, and a well-defined marker of synaptopathy (Sergeyenko,
275 Lall, Liberman, & Kujawa, 2013). We found no differences in CtBP-2 labeled
276 synaptic boutons of IHC in the three cochlea turns between WT and Spnb5$^{(-/-)}$ mice
277 (**Figure 5I**). We then sought to identify morphological differences in afferent nerve
278 numbers as a possible cause of the reduced wave I amplitudes. We found
279 significant reductions in neurofilament labeled, nonmyelinated, afferent fibers in
280 the habenular in all three turns as well as efferent fibers in the basal and middle
281 turns of the cochlea (**Figure 5G, H**).

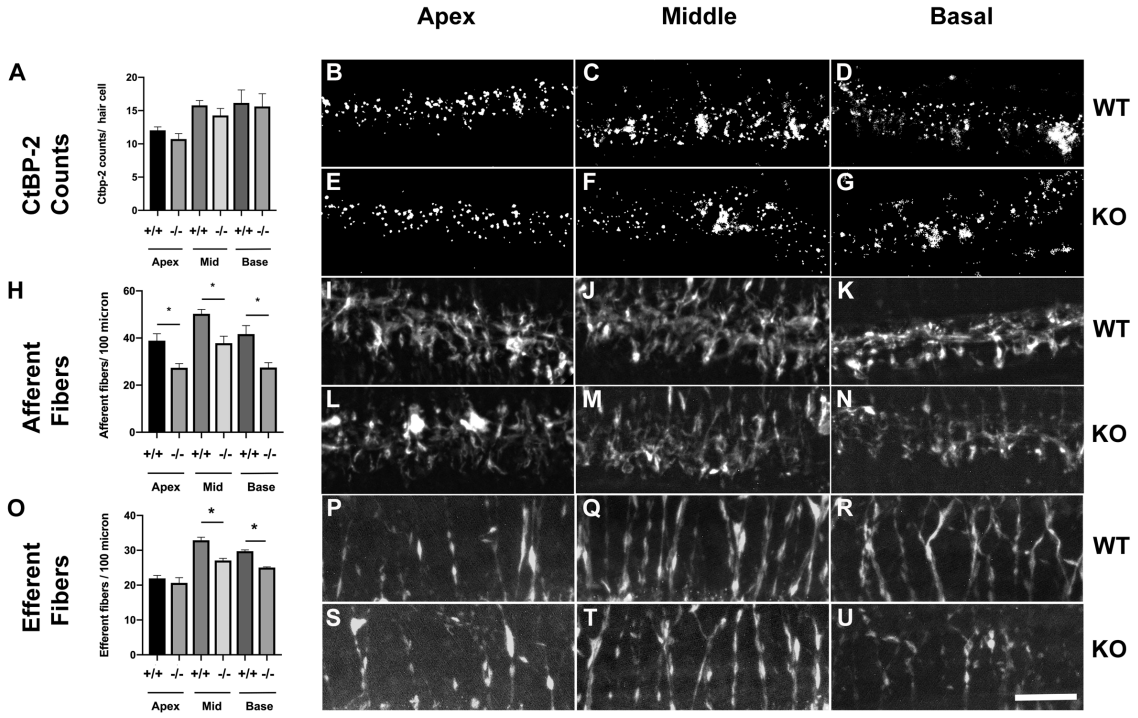

282 **Figure 5**

283 **Figure 5. Spnb5$^{(-/-)}$ mice show evidence of neuropathy and no evidence of a synaptopathy.**
284 Shown are representative z axis projections of confocal micrographs of WT and βV spectrin KO
285 mice in which synaptic boutons are labeled with antibodies to CtBP-2 (**B-G**). **Afferent (I-N) and**
286 **efferent (P-U) nerve fibers are labeled with antibodies to neurofilament.** The scale bar

287 equates to 20 microns. There is a significant reduction in the density of afferent fibers at the
288 habenular in all three turns and efferent fibers in the cochlear canal of Spnb5$^{(-/-)}$ mice. In contrast,
289 there were no differences in CtBP-2 positive bouton counts in all three turns of the cochlea. (**A, H,**
290 **O) Shown are the mean (+/- SEM) synaptic (A) counts, afferent (H) and efferent (O) neuronal**
291 **and in all three turns of the cochlea.** The differences in afferent and efferent counts were
292 significant (* $P<0.05$, n = 4 cochlea) between WT and Spnb5$^{(-/-)}$ mice in all three turns of the cochlea
293 (afferent), and in the middle and basal turns of the cochlea (efferent). CtBP-2 counts between WT
294 and Spnb5$^{(-/-)}$ mice were not significantly different ($P>0.05$).
295

296 **DISCUSSION**

297 In this paper, we elucidate the function of βV spectrin in hearing using a mouse
298 gene deletion model. Removal of exon 2 containing the initiator methionine and an
299 N-terminal 37 amino acids, which, in part, compose its actin-binding domain,
300 results in a mouse with normal ABR thresholds, and normal measures of OHC
301 function including DPOAE and NLC. Typical DPOAEs are a strong indication of
302 normal OHC electromotility (Shera & Guinan, 1999). The presence of normal NLC
303 measures further reiterates this interpretation. Moreover, we were unable to detect
304 Spnb5 mRNA in the organ of Corti or OHCs.
305

306 In contrast, we find a reduction in wave I amplitudes that are concordant with our
307 finding of reduced numbers of nerve fibers. These data point to βV spectrin as
308 critical for the maintenance and function of afferent and efferent nerve fibers. The
309 normal ABR thresholds in the presence of reduced wave I amplitudes we observe
310 in mice have been seen previously in mutations of other proteins and, in particular,
311 in the recovery phase of noise-induced hearing loss (Maison, Pyott, Meredith, &
312 Liberman, 2013) (Kujawa & Liberman, 2009).
313

314 How do we explain the preserved ABR thresholds in the presence of reduced wave
315 I amplitudes? Loss of neurons of up to 80% has been shown to be associated with
316 normal thresholds as long as hair cells were functional (Schuknecht & Woellner,
317 1953). Although speculative, other authors have reasoned that a small increase in
318 sound pressure of 5 dB results in wider recruitment of neurons adjacent to the
319 index sound frequency that could compensate for a 50% loss in afferent neurons
320 using insensitive measures such as compound action potentials and ABRs
321 (Taberner and Liberman 2005), (Lin, Furman, Kujawa, & Liberman, 2011). An
322 important distinction in our data is that, unlike in noise-induced hearing loss
323 models, we see no differences in CtBP-2 counts (Liberman & Kujawa, 2017). Our
324 CtBP-2 counts and preliminary analysis using nerve counts suggest that the
325 functional effects in these mice lie in the nerve. Ongoing work in our lab includes
326 detailed analysis of high and low threshold fiber counts in these animals, together
327 with studies that will better determine the exact molecular mechanisms which
328 underlie the reduction in dendritic and axonal numbers.
329
330 We find absent effects on OHC function in Spnb5$^{(-/-)}$ mice that is consistent with
331 the undetectable expression of these transcripts in the cochlea and OHC in
332 particular. We note similar low/absent Spnb5 RNA expression upon interrogation
333 of both OHC single-cell RNA and OHC RNA expression datasets of adult mice that
334 have been published (Li et al., 2018) and gEAR portal (Shen, Scheffer, Kwan, &
335 Corey, 2015), (Liu, Chen et al. 2018), (Hoa et al., 2020). Together, these data
336 question the validity of βV spectrin antibody staining of OHCs, the principal reason

337 for ascribing its presence in OHCs (Legendre et al., 2008), (Cortese et al., 2017).
338 These papers led to the belief that βV spectrin had an integral role in the
339 cytoskeleton of hair cells. Our assertion that βV spectrin is not important for OHC
340 function is based, in part, on the absent phenotype in the knockout mice. It is
341 reasonable to ask if the knockout mouse resulted in an actual loss of function in
342 the gene. We feel confident that the deletion of the second exon in Spnb5$^{(-/-)}$
343 resulted in a silencing of the gene. In addition to the neuronal phenotype we
344 describe herein with the Spnb5$^{(-/-)}$ mice, we were also unable to detect Spnb5
345 transcript from the testis of knockout mice that may relate to degradation of
346 nonsense transcripts and a phenomenon observed in deletion of other genes
347 (Baker & Parker, 2004). While the phenotype of mice is consistent with the absent
348 expression of Spnb5 transcript in OHCs, we have to be mindful that normal OHC
349 function in these mice could be due to other beta spectrins substituting for Spnb5
350 spectrin. In this context, the presence of a clear auditory phenotype in the Spnb2
351 spectrin knockout mice would suggest that such an interchange and substitution
352 by other spectrins is, however, not likely. Moreover, Spnb4$^{(qv/qv)}$ spectrin has a
353 neuronal phenotype, similar to Spnb5$^{(-/-)}$.
354
355 In conclusion, we present data in this study that βV spectrin plays an important role
356 in auditory function. Our data confirm that βV spectrin is necessary to maintain the
357 integrity or function of afferent and efferent nerves of the peripheral auditory
358 system. Importantly, our data show no evidence that βV spectrin has a function in
359 OHCs, as has been previously suggested.

360 **MATERIALS AND METHODS**

361 **Mice.**

362 All procedures conducted with mice were approved by the Institutional Animal Care
363 and Use Committee at the Yale University School of Medicine. C57BL/6J mice
364 were housed under pathogen-free conditions and maintained as a breeding
365 colony. In our studies, C57BL/6J mice were engineered to harbor a gene knockout
366 of Spnb5 (βV spectrin). The floxed exon 2 of Spnb5 was excised with Cre-
367 recombinase from embryonic stem (ES) cells in culture before injecting them into
368 mouse blastocysts under the guidance of the Yale Gene Targeting Center. This
369 construct was designed to create a constitutive loss of βV spectrin. For genotyping
370 animals, tail snips were collected from mice at their weaning age. Genomic DNA
371 was prepared by an overnight 56˚C incubation in tail lysis buffer 50mM Tris pH 8.0,
372 50mM KCL, 2.5mM EDTA, 0.4% Igepal, 0.4% Tween20 supplemented with
373 Proteinase K (400 μg/ml). gDNA was assayed by PCR using the following primer
374 set: Forward 5'-CTGTCCGCCAAAGAGCAGGGGCCATG-3' Reverse 5'-
375 GATGTGGGGTCAGCCCAGCATCTCC-3' and PCR amplimers were visualized
376 on a 2% agarose gel.

377

378 **Organ of Corti and OHC isolation.**

379 Prestin-YFP mice that were 2-3 months old were euthanized and the cochleae
380 extracted. The organ of Corti was dissected and treated with pre-warmed 0.05%
381 trypsin for 8 minutes at 37˚C. The organ of Corti was dissociated by triturating the
382 tissue 20-30 times in a 1 ml pipet tip. The cell suspension was spun at 1500 g for

383 10 minutes. The cell pellet was resuspended in DMEM supplemented with 10%
384 FBS and then filtered through a 40-micron cell strainer. The cells were FACS
385 sorted, and YFP positive OHCs were collected.
386
387 **mRNA detection.**
388 Total RNA from mouse testis and the whole brain was either obtained from Takara
389 or prepared from 100 mg of testis tissue from 3 month WT and βV KO C57BL/6J
390 animals with Trizol reagent (Chomczynski & Mackey, 1995). cDNA was prepared
391 with Superscript IV reverse transcriptase (ThermoFisher Scientific, Waltham, MA,)
392 and quantified with a Nanodrop spectrophotometer. Standard procedures followed
393 reagent manufactures directions for first-strand synthesis. The organ of Corti and
394 OHCs (prepared as described above) were isolated and proteolyzed with 1 unit of
395 proteinase K. After inactivating at 95˚C for 5 minutes, non-purified RNA was
396 treated with Superscript IV to generate cDNA. Gene-specific PCR primers bridging
397 consecutive exons were designed to ensure the exclusion of genomic DNA from
398 amplification in **Table 1**.
399
400 **Auditory brainstem responses (ABR).**
401 ABR experiments were conducted in a manner similar to that described by Song
402 *et. al.* (El-Hassar et al., 2019). Briefly, animals were anesthetized with 480 mg/kg,
403 i.p., chloral hydrate, and all recordings were conducted in a sound-attenuating
404 chamber (Industrial Acoustics Corp., Bronx, NY). A customized TDT3 system
405 (Tucker-Davis Technologies Inc., Alachua, FL) was used for ABR recordings.

406 Subdermal needle electrodes (Rochester Electro-Medical, Lutz, FL) were
407 positioned at the vertex (active, noninverting), the infra-auricular mastoid region
408 (reference, inverting), and the neck region (ground). Differentially recorded scalp
409 potentials were bandpass filtered between 0.05 and 3 kHz over a 15 ms epoch. A
410 total of 400 trials was averaged for each waveform for each stimulus condition.
411
412 Symmetrically shaped tone bursts were 3 ms long (1 ms raised cosine on/off ramps
413 and 1 ms plateau). All acoustic stimuli were delivered free field via a speaker (Part
414 FF1 2021, Tucker-Davis Technologies) positioned 10 cm from the vertex. Stimulus
415 levels were calibrated using a 0.5-inch condenser microphone (model 4016, ACO
416 Pacific, Belmont, CA) positioned at the approximate location of the animal's head
417 during recording sessions and are reported in decibels of sound pressure level
418 (SPL; referenced to 20 μPa). Stimuli of alternating polarity were delivered at a rate
419 of ~20/s. Tone burst responses were collected in half-octave steps ranging from
420 32 to 2.0 kHz. The effects of the level were determined by decreasing stimulus
421 intensity in 5 dB steps up to a maximum stimulus level of 90 dB SPL. The ABR
422 threshold was defined as the lowest intensity of sound level capable of evoking a
423 reproducible, visually detectable response. Latencies and amplitudes of the initial
424 ABR peaks were measured from sound stimuli delivered at a rate of 20/s and at a
425 frequency of 16 kHz, one of the most sensitive frequency ranges of hearing in
426 mice. Latencies and amplitudes of wave I at 90 dB SPL were also measured at all
427 the other frequencies. The analysis was performed in BioSig software (BioSig
428 Technologies, Westport, CT) on traces with discernible peaks by setting cursors

429 at the maxima and minima of the peaks. Latency was defined as the time from the
430 onset of the stimulus to the peak, while amplitude was measured by taking the
431 mean of the ΔV of the positive and negative deflections of the ABR wave.
432
433 **Distortion product otoacoustic emissions (DPOAE).**
434 The acoustic stimuli were produced, and responses were recorded using a
435 customized TDT3 system (Tucker-Davis Technologies Inc., Alachua, FL)
436 controlled by BioSig, digital signal processing software. DPOAE was measured
437 by inserting a probe into anesthetized mouse external ear canal to deliver sound
438 stimuli, and emissions of sound were collected by a microphone and recorded for
439 subsequent analysis. To deliver acoustic stimuli and record the responses, two
440 speakers (f_1 and f_2) (MF1 Multi-Field Magnetic Speakers, TDT) and a microphone
441 (ER-10B, Etymotic Research, Elk Grove Village, IL) were connected to a short
442 PVC tube, and tapered plastic probe that was inserted into the external auditory
443 meatus of the mice. Two simultaneous continuous pure tones (f_1 and f_2) that have
444 a frequency ratio of 1.2 (f_2/f_1) and equal sound level ($L_1 = L_2$) were delivered at
445 center frequencies of 8, 12, 16, 24 and 32 kHz with sound levels from 80 to 20 dB
446 SPL in 10 dB decrements. Stimuli duration was 83.88 ms at a repetition rate of
447 11.92 per second. The acquired DPOAE responses were averaged 100 times. The
448 DPOAE of interest was at $2f_1$-f_2, the largest and most prominent DPOAE. The
449 DPOAE threshold was defined as the lowest sound intensity capable of evoking a
450 visually detectable $2f_1$-f_2 signal above the noise floor. DPOAE amplitudes were
451 analyzed offline in BioSigRP by setting cursors at the peak of the $2f_1$-f_2 signals.

452

453 **Nonlinear capacitance (NLC).**

454 Nonlinear capacitance was conducted in a fashion much like that previously
455 described in the Methods Mol. Biol. 2016 Song and Santos-Sacchi (Song &
456 Santos-Sacchi, 2016). WT C57BL/6J and βV spectrin KO littermates at postnatal
457 day 13 and at 2-month-old were compared. Apical turns of the organ of Corti were
458 isolated from each and recorded with ionic current blocking solutions to minimize
459 interference on measures of membrane capacitance. The extracellular solution
460 contained (in mM): 100 NaCl, 20 tetraethylammonium (TEA)-Cl, 20 CsCl, 2 $CoCl_2$,
461 1 $MgCl_2$, 1 $CaCl_2$, 10 HEPES, pH 7.2. The intracellular solution contained (in mM):
462 140 CsCl, 2 $MgCl_2$, 10 HEPES, and 10 EGTA, pH 7.2. Pipettes had resistances of
463 3-5 MΩ. Gigohm seals were made, and stray capacitance was balanced out with
464 amplifier circuitry prior to establishing whole-cell conditions. A Nikon Eclipse E600-
465 FN microscope with 40× water immersion objective lens was used to observe cells
466 during voltage clamp. Whole-cell voltage-clamp recordings were performed from
467 all three rows of OHCs on whole-mount organ of Corti. OHCs were recorded at
468 room temperature using jClamp software and an Axopatch 200B amplifier. Data
469 were low pass filtered at 10 kHz and digitized at 100 kHz with a Digidata 1320A.
470 In order to extract Boltzmann parameters, capacitance-voltage data were fit to the
471 first derivative of a two-state Boltzmann function.

472

473

474 $$C_m = NLC + C_{sa} + C_{\text{lin}} = Q_{\text{max}} \frac{\text{ze}}{k_B T} \frac{b}{(1+b)^2} + C_{sa} + C_{\text{lin}} \quad \text{(eq.1)}$$

475

476

477 where $b = exp\left(-ze\frac{V_m - V_h}{k_B T}\right)$, $C_{sa} = \frac{\Delta C_{sa}}{(1+b^{-1})}$

478

479 Q_{max} is the maximum nonlinear charge moved, V_h is the voltage at peak
480 capacitance or equivalently, at half-maximum charge transfer, V_m is Rs-corrected
481 membrane potential, z is valence, C_{lin} is linear membrane capacitance, e is the
482 electron charge, kB is Boltzmann's constant, and T is the absolute temperature.

483

484 **Immunocytochemistry (ICC).**

485 For ICC, staining was performed on fixed and decalcified 3 turns of the organ of
486 Corti to compare the number of neuronal fibers and synapses between all 3 turns
487 organ of Corti in KO and WT mice. Temporal bones were fixed overnight in 4˚C
488 and then decalcified in 120 mM ethylenediaminetetraacetic acid (EDTA) for 2 days.
489 Whole-mount of the organ of Corti was dissected, washed in PBS 0.05% Tween
490 20, 0.05% Triton-X 100 (incubation buffer) three times for 3 minutes, and incubated
491 with primary antibody in incubation buffer overnight at 4˚C with mouse anti-CtBP-
492 2 antibody (1:50, BD Transduction, San Jose, CA, cat# 612044), chicken anti-
493 neurofilament (NF) antibody (1:500, MilliporeSigma, Billerica, MA, cat# AB5539).
494 After three washes in incubation buffer, the tissue was incubated with secondary
495 antibody in incubation buffer for 1 hour at room temperature. The secondary
496 antibodies used included donkey anti-rabbit Alexa Fluor 568/647 (1:200; Thermo
497 Fisher Scientific, cat # A-10042/A-31573), goat anti-mouse Alexa Fluor
498 568/647 (1:200; Thermo Fisher Scientific, cat # A-21124/A-21235) and goat anti-
499 chicken Alexa Fluor 488/594 (1:200; Thermo Fisher Scientific, cat # A-11039/A-
500 11042). After antibody treatment, cells were washed in incubation buffer and

501 mounted in Vectashield (Vector Laboratories, Inc., Burlingame, CA), and viewed
502 using a Zeiss confocal laser-scanning microscope (Oberkochen, Germany).
503
504 Nerve (NF positive) and synaptic vesicle (CtBP-2 positive) counts were performed
505 posthoc in Fiji (ImageJ). Briefly, z stacks of images were separated by probes,
506 background-subtracted (using a 50-pixel rolling ball radius), and z sections
507 containing the images of interest identified for further analysis (slice keeper). CtBP-
508 2 labeled IHCs and NF labeled afferent fibers surrounding IHCs in proximity to the
509 habenula and efferent fibers in the cochlear canal were counted. Z projections
510 (sum) of the respective sections were obtained and automated thresholds
511 determined (max entropy). Counts of particles (synaptic vesicles) immunopositive
512 for CtBP-2 larger than 0.1 microns were scored. Neuronal numbers were
513 established by counting the peaks in a profile plotted perpendicular to neural fibers
514 in the cochlea canal. For afferent nerve counts the profile was plotted at the
515 midpoint of nerve densities.
516
517 **Statistical Analysis**.
518 Data were analyzed using FIJI, Microsoft Excel, SigmaPlot and GraphPad Prism.
519 The measures of variability are depicted as error bars +/- the SEM and stated
520 numerically in the figure legends. Unpaired, one or two-tailed Student's t-test were
521 performed using both Excel and GraphPad Prism to make comparisons between
522 WT and Spnb5$^{(-/-)}$ data points. P-values are indicated in the figure legends to two
523 significant figures. The sample size (n) is stated in the figures.

524

525 **COMPETING INTERESTS**

526 The authors declare no competing interests.

527

528 **AUTHOR CONTRIBUTIONS**

529 MCS, JPB, JSM, DN and JSS conceptualized the project. PRS and JSM
530 generated the Spnb5 deleted mice. MCS and JPB conducted animal breeding and
531 genotyping. MCS, JPB, SK, and DN performed gene expression and
532 immunohistochemistry analysis. JPB and LS performed assays to assess hearing
533 function. MCS and DN wrote the manuscript, and all authors contributed to its
534 editing and refinement.

535

536 **ACKNOWLEDGEMENTS**

537 These studies were supported by grants R01 DC 008130 and R01 DC 008130
538 from the National Institute of Health to JSS and DN and grants P01 NS35476
539 (project 4) and R01 HL28560 to JSM. Other support includes the Raymond Yesner
540 Endowment to Yale University (JSM). We also would like to thank Winston Tan,
541 Alexei Surguchev and Lan Ji for their technical assistance.

542

REFERENCES

Abe, T., Kakehata, S., Kitani, R., Maruya, S., Navaratnam, D., Santos-Sacchi, J., & Shinkawa, H. (2007). Developmental expression of the outer hair cell motor prestin in the mouse. *J Membr Biol, 215*(1), 49-56. doi:10.1007/s00232-007-9004-5

Bai, J. P., Surguchev, A., Ogando, Y., Song, L., Bian, S., Santos-Sacchi, J., & Navaratnam, D. (2010). Prestin surface expression and activity are augmented by interaction with MAP1S, a microtubule-associated protein. *J Biol Chem, 285*(27), 20834-20843. doi:10.1074/jbc.M110.117853

Baker, K. E., & Parker, R. (2004). Nonsense-mediated mRNA decay: terminating erroneous gene expression. *Curr Opin Cell Biol, 16*(3), 293-299. doi:10.1016/j.ceb.2004.03.003

Benson, D. A., Cavanaugh, M., Clark, K., Karsch-Mizrachi, I., Lipman, D. J., Ostell, J., & Sayers, E. W. (2013). GenBank. *Nucleic Acids Res, 41*(Database issue), D36-42. doi:10.1093/nar/gks1195

Bramhall, N. F., McMillan, G. P., Kujawa, S. G., & Konrad-Martin, D. (2018). Use of non-invasive measures to predict cochlear synapse counts. *Hear Res, 370*, 113-119. doi:10.1016/j.heares.2018.10.006

Chomczynski, P., & Mackey, K. (1995). Short technical reports. Modification of the TRI reagent procedure for isolation of RNA from polysaccharide- and proteoglycan-rich sources. *Biotechniques, 19*(6), 942-945. Retrieved from https://www.ncbi.nlm.nih.gov/pubmed/8747660

Consortium, G. T. (2013). The Genotype-Tissue Expression (GTEx) project. *Nat Genet, 45*(6), 580-585. doi:10.1038/ng.2653

Cortese, M., Papal, S., Pisciottano, F., Elgoyhen, A. B., Hardelin, J. P., Petit, C., . . . El-Amraoui, A. (2017). Spectrin betaV adaptive mutations and changes in subcellular location correlate with emergence of hair cell electromotility in mammalians. *Proc Natl Acad Sci U S A, 114*(8), 2054-2059. doi:10.1073/pnas.1618778114

Efimova, N., Korobova, F., Stankewich, M. C., Moberly, A. H., Stolz, D. B., Wang, J., . . . Svitkina, T. (2017). betaIII Spectrin Is Necessary for Formation of the Constricted Neck of Dendritic Spines and Regulation of Synaptic

576 Activity in Neurons. *J Neurosci, 37*(27), 6442-6459.
577 doi:10.1523/JNEUROSCI.3520-16.2017

578 El-Hassar, L., Song, L., Tan, W. J. T., Large, C. H., Alvaro, G., Santos-Sacchi, J.,
579 & Kaczmarek, L. K. (2019). Modulators of Kv3 Potassium Channels
580 Rescue the Auditory Function of Fragile X Mice. *J Neurosci, 39*(24), 4797-
581 4813. doi:10.1523/JNEUROSCI.0839-18.2019

582 Hafidi, A., Despres, G., & Romand, R. (1990). Cochlear innervation in the
583 developing rat: an immunocytochemical study of neurofilament and
584 spectrin proteins. *J Comp Neurol, 300*(2), 153-161.
585 doi:10.1002/cne.903000202

586 Hammarlund, M., Jorgensen, E. M., & Bastiani, M. J. (2007). Axons break in
587 animals lacking beta-spectrin. *J Cell Biol, 176*(3), 269-275.
588 doi:10.1083/jcb.200611117

589 Hoa, M., Olszewski, R., Li, X., Taukulis, I., Gu, S., DeTorres, A., . . . Kelley, M.
590 W. (2020). Characterizing Adult Cochlear Supporting Cell Transcriptional
591 Diversity Using Single-Cell RNA-Seq: Validation in the Adult Mouse and
592 Translational Implications for the Adult Human Cochlea. *Front Mol*
593 *Neurosci, 13*, 13. doi:10.3389/fnmol.2020.00013

594 Holley, M. C., & Ashmore, J. F. (1990). Spectrin, actin and the structure of the
595 cortical lattice in mammalian cochlear outer hair cells. *J Cell Sci, 96 (Pt*
596 *2)*, 283-291. Retrieved from http://www.ncbi.nlm.nih.gov/pubmed/2211870

597 Holley, M. C., Kalinec, F., & Kachar, B. (1992). Structure of the cortical
598 cytoskeleton in mammalian outer hair cells. *J Cell Sci, 102 (Pt 3)*, 569-
599 580. Retrieved from https://www.ncbi.nlm.nih.gov/pubmed/1506434

600 Kujawa, S. G., & Liberman, M. C. (2009). Adding insult to injury: cochlear nerve
601 degeneration after "temporary" noise-induced hearing loss. *J Neurosci,*
602 *29*(45), 14077-14085. doi:10.1523/JNEUROSCI.2845-09.2009

603 Legendre, K., Safieddine, S., Kussel-Andermann, P., Petit, C., & El-Amraoui, A.
604 (2008). alphaII-betaV spectrin bridges the plasma membrane and cortical
605 lattice in the lateral wall of the auditory outer hair cells. *J Cell Sci, 121*(Pt
606 20), 3347-3356. doi:10.1242/jcs.028134

Lewis, M. A., Nolan, L. S., Cadge, B. A., Matthews, L. J., Schulte, B. A., Dubno, J. R., . . . Dawson, S. J. (2018). Whole exome sequencing in adult-onset hearing loss reveals a high load of predicted pathogenic variants in known deafness-associated genes and identifies new candidate genes. *BMC Med Genomics, 11*(1), 77. doi:10.1186/s12920-018-0395-1

Li, Y., Liu, H., Giffen, K. P., Chen, L., Beisel, K. W., & He, D. Z. Z. (2018). Transcriptomes of cochlear inner and outer hair cells from adult mice. *Sci Data, 5*, 180199. doi:10.1038/sdata.2018.199

Liberman, M. C., & Kujawa, S. G. (2017). Cochlear synaptopathy in acquired sensorineural hearing loss: Manifestations and mechanisms. *Hear Res, 349*, 138-147. doi:10.1016/j.heares.2017.01.003

Lin, H. W., Furman, A. C., Kujawa, S. G., & Liberman, M. C. (2011). Primary neural degeneration in the Guinea pig cochlea after reversible noise-induced threshold shift. *J Assoc Res Otolaryngol, 12*(5), 605-616. doi:10.1007/s10162-011-0277-0

Liu, Y., Qi, J., Chen, X., Tang, M., Chu, C., Zhu, W., . . . Zhong, G. (2019). Critical role of spectrin in hearing development and deafness. *Sci Adv, 5*(4), eaav7803. doi:10.1126/sciadv.aav7803

Lorenzo, D. N., Badea, A., Zhou, R., Mohler, P. J., Zhuang, X., & Bennett, V. (2019). betaII-spectrin promotes mouse brain connectivity through stabilizing axonal plasma membranes and enabling axonal organelle transport. *Proc Natl Acad Sci U S A, 116*(31), 15686-15695. doi:10.1073/pnas.1820649116

Maison, S. F., Pyott, S. J., Meredith, A. L., & Liberman, M. C. (2013). Olivocochlear suppression of outer hair cells in vivo: evidence for combined action of BK and SK2 channels throughout the cochlea. *J Neurophysiol, 109*(6), 1525-1534. doi:10.1152/jn.00924.2012

Melcher, J. R., Knudson, I. M., Fullerton, B. C., Guinan, J. J., Jr., Norris, B. E., & Kiang, N. Y. (1996). Generators of the brainstem auditory evoked potential in cat. I. An experimental approach to their identification. *Hear Res, 93*(1-2), 1-27. doi:10.1016/0378-5955(95)00178-6

Papal, S., Cortese, M., Legendre, K., Sorusch, N., Dragavon, J., Sahly, I., . . . El-Amraoui, A. (2013). The giant spectrin betaV couples the molecular

motors to phototransduction and Usher syndrome type I proteins along their trafficking route. *Hum Mol Genet, 22*(18), 3773-3788. doi:10.1093/hmg/ddt228

Parkinson, N. J., Olsson, C. L., Hallows, J. L., McKee-Johnson, J., Keogh, B. P., Noben-Trauth, K., . . . Tempel, B. L. (2001). Mutant beta-spectrin 4 causes auditory and motor neuropathies in quivering mice. *Nat Genet, 29*(1), 61-65. doi:10.1038/ng710

Schuknecht, H. F., & Woellner, R. C. (1953). Hearing losses following partial section of the cochlear nerve. *Trans Am Laryngol Rhinol Otol Soc, 58*(57th Meeting), 369-393; discussion, 393-364. Retrieved from https://www.ncbi.nlm.nih.gov/pubmed/13146770

Sergeyenko, Y., Lall, K., Liberman, M. C., & Kujawa, S. G. (2013). Age-related cochlear synaptopathy: an early-onset contributor to auditory functional decline. *J Neurosci, 33*(34), 13686-13694. doi:10.1523/JNEUROSCI.1783-13.2013

Shen, J., Scheffer, D. I., Kwan, K. Y., & Corey, D. P. (2015). SHIELD: an integrative gene expression database for inner ear research. *Database (Oxford), 2015*, bav071. doi:10.1093/database/bav071

Shera, C. A., & Guinan, J. J., Jr. (1999). Evoked otoacoustic emissions arise by two fundamentally different mechanisms: a taxonomy for mammalian OAEs. *J Acoust Soc Am, 105*(2 Pt 1), 782-798. doi:10.1121/1.426948

Song, L., McGee, J., & Walsh, E. J. (2006). Frequency- and level-dependent changes in auditory brainstem responses (ABRS) in developing mice. *J Acoust Soc Am, 119*(4), 2242-2257. doi:10.1121/1.2180533

Song, L., & Santos-Sacchi, J. (2016). A Walkthrough of Nonlinear Capacitance Measurement of Outer Hair Cells. *Methods Mol Biol, 1427*, 501-512. doi:10.1007/978-1-4939-3615-1_28

Stabach, P. R., & Morrow, J. S. (2000). Identification and characterization of beta V spectrin, a mammalian ortholog of Drosophila beta H spectrin. *J Biol Chem, 275*(28), 21385-21395. doi:10.1074/jbc.C000159200

670 Stankewich, M. C., Cianci, C. D., Stabach, P. R., Ji, L., Nath, A., & Morrow, J. S.
671 (2011). Cell organization, growth, and neural and cardiac development
672 require alphaII-spectrin. *J Cell Sci, 124*(Pt 23), 3956-3966.
673 doi:10.1242/jcs.080374

674 Stankewich, M. C., Gwynn, B., Ardito, T., Ji, L., Kim, J., Robledo, R. F., . . .
675 Morrow, J. S. (2010). Targeted deletion of betaIII spectrin impairs
676 synaptogenesis and generates ataxic and seizure phenotypes. *Proc Natl*
677 *Acad Sci U S A, 107*(13), 6022-6027. doi:10.1073/pnas.1001522107

678 Yue, F., Cheng, Y., Breschi, A., Vierstra, J., Wu, W., Ryba, T., . . . Mouse, E. C.
679 (2014). A comparative encyclopedia of DNA elements in the mouse
680 genome. *Nature, 515*(7527), 355-364. doi:10.1038/nature13992
681
682

Table1. Beta spectrin gene specific primers.

Primers					Amplimer (bps)
Spnb1	forward	CAAAGAGCAGGAGGTGTCAGC	reverse	TCTAGGCAGGTGCTGAAGTTC	264
	nested forward	GATGCGTGTGCCGGGCGCC	nested reverse	CTGGTATTGATCTCTGCCT	197
Spnb2	forward	CCGGTGGGAGTGGTTAAGAC	reverse	CATCCCAGGTCGCTGCAGAC	188
	nested forward	GATTTTGGAGGTCCATCAG	nested reverse	TCAAACGCCTCATGGCGCT	144
Spnb5	forward	CTCCGGAGCTTTGAGCAGGCTGC	reverse	CCTGAGCCCACGCTAGCAATTCC	439
	nested forward	GATACAGGAGAAGACCACC	nested reverse	TTCCTGGACTTTGGCCTCC	319
Spnb5	forward	TGGCCTTCCTCAGGGCCAAGGT	reverse	GCACTCATCTGGATGCAGGGCTG	440
	nested forward	CTTGGACAGGGAGGAGTTTGG	nested reverse	GCACTCATCTGGATGCAGGGCTG	313

Primer sets were used to detect for mRNA of Spnb1, Spnb2, and Spnb5 in the brain, organ of Corti, and isolated OHCs. The PCR amplimer sizes from mRNA are presented in the final column.

Table 2. Primers for the Spnb5 gene used to prepare the three DNA fragments that were subcloned into pEasy-Flox.

Fragment 1	forward	CAGCGGCCGCAGGGGCTGCCTCCTACTGTACC	reverse	GAGCGGCCGCACTTGAATGACCCAGAGCCACCCCT
Fragment 2	forward	GGTCTAGACCTCTTACTCGCTTAGGTTCCAATC	reverse	GCTCTAGATGACTCTACAGCAGACCCCCAGGTC
Fragment 3	forward	GACTCGAGCCTGTAGCTATTTCTGGCCTACCCCTCC	reverse	GACTCGAGGGAGGGAGGGTTACTGTAGTAGAAGGGC

The targeting vector for homologous recombination was constructed by cloning three PCR generated fragments into the pEASY-Flox vector. Fragment 1 is a 4115 bp product, fragment 2 is a 469 bp product that contains Spnb5 exon 2, and fragment 3 is 4371 bp of sequence that spans up to exon 5. The three fragments were sequence verified. The oligos contain common restriction sites at their 5' end for easy cloning into the targeting vector.

Table 3. Primers for rt-PCR in WT and Spnb5$^{(-/-)}$ tissue.

Spnb5	exon 58/60	forward	CTCCGGAGCTTTGAGCAGGCTGC	reverse	CCTGAGCCCACGCTAGCAATTCC	439
Spnb5	exon 53/55	forward	AGGAGAAACACCAGAATTTGGAGAATG	reverse	TGTCCACTCTCCAGAAGGGCAACTG	412
Spnb2	exon 28/29	forward	GATACAGGAGAAGACCACC	reverse	TTCCTGGACTTTGGCCTCC	144
Spna2	exon 54/55	forward	AACAGGAGTGACTGAGGAGG	reverse	CCTTCCTCAACCATTGGCAGA	144

These primer sets were tested on cDNA from testis isolated from WT and Spnb5$^{(-/-)}$ 3-month-old mice. Because the C-terminus of these large genes tends to be more abundant than N-terminus exons, we designed primer sets that will amplify exons near the poly-A tail.